Micron 205 (2026) 104048

Contents lists available at ScienceDirect

Micron

journal homepage: www.elsevier.com/locate/micron

Full length article

Crystallographically controlled alignment of melt inclusion entrapment in magmatic olivine: Insights from Lab-Diffraction Contrast Tomography

Helen Thornhill [a,*], Patrick Trimby [b], Gareth Douglas [c], Alice Macente [d], David Ferguson [a], Felix Boschetty [e]

[a] Institute of Geophysics and Tectonics, School of Earth and Environment, University of Leeds, LS2 9JT, UK
[b] Carl Zeiss Ltd. Zeiss House, Cambourne Business Park, Cambridge, UK
[c] School of Engineering, University of Leicester, UK
[d] Department of Earth Sciences, University of Florence, Italy
[e] Department of Earth Sciences, Oxford University, UK

ARTICLE INFO

Keywords:
LabDCT
Melt inclusions
Olivine
X-ray computed tomography
3D crystallography
Microstructure

ABSTRACT

Laboratory Diffraction Contrast Tomography (LabDCT) is a recent analytical development that allows for non-destructive microstructural characterisation of crystalline materials using a laboratory-scale X-ray microscope. In this study, we apply LabDCT to investigate magmatic olivine crystals hosting melt inclusion populations with preferential alignment. Melt inclusions provide valuable insights into magmatic and volcanic processes, and are often the subject of extensive geochemical investigation. Destructive sample preparation can prematurely erase contextural information such as inclusion geometries, population characteristics, and the relationship between the inclusion and its host crystal. The approach used in this study shows a clear crystallographic control on melt inclusion orientations where a visual alignment is identified. Melt inclusions consistently align parallel with the a-axis ([100]) of their olivine hosts. This alignment suggests that inclusion entrapment occurred during rapid, skeletal olivine growth, likely the result of thermal disequilibrium and undercooling within the magmatic system. This insight was gained without destructive sample preparation, highlighting the value of these X-ray imaging techniques for microstructural investigation and sample characterisation. This study demonstrates the range of opportunities available by applying non-destructive, three-dimensional X-ray imaging techniques to investigate geomaterials. The method described and applied in this study can be used to compare the orientation of any internal feature to its mineral host, such as melt inclusions and their host olivine crystals.

1. Introduction

Understanding the spatial distribution of minerals and inclusions within natural materials is crucial for interpreting geological processes, and predicting their physical behaviour and properties. Natural silicate minerals commonly contain internal inclusions, trapped during mineral growth in geological environments. These inclusions can be composed of a variety of materials, such as other mineral phases, fluids, and silicate melt. These can reveal valuable insights into the geological processes that occur within the Earth, however their utility is often limited by a lack of three-dimensional spatial and microstructural context. Microstructure, the internal structure of a material at the microscopic scale, is commonly analysed, visualised and quantified in two dimensions, using techniques such as Electron Back-scatter Diffraction (EBSD) analysis (Prior et al., 1999; Humphreys, 2004; Kahl et al., 2017; Wieser et al., 2020). EBSD is a technique that uses a Scanning Electron Microscope (SEM), exploiting the interaction between back-scattered electrons and the surface of a polished, tilted sample. A focused electron beam interacts with the crystal lattice, generating diffraction patterns that can be indexed to determine the crystal structure and its absolute orientation (Prior et al., 1999). In this way, the surface of a material can be analysed, however this can only reveal two-dimensional information.

To extend this technique to three dimensions, EBSD can be coupled with Focused Ion Beam (FIB) milling (Matteson et al., 2002; Xu et al., 2007; Wirth, 2009). In this approach, an ion beam (commonly Ga^+), is focused onto the surface of a sample to selectively mill away material with <10 nm precision. The surface quality is sufficient that the exposed surface can then be analysed using conventional EBSD analysis. Further milling can remove predefined thicknesses of material

* Corresponding author.
E-mail address: ee18hrt@leeds.ac.uk (H. Thornhill).

https://doi.org/10.1016/j.micron.2026.104048
Received 26 January 2026; Received in revised form 11 May 2026; Accepted 18 May 2026
Available online 22 May 2026

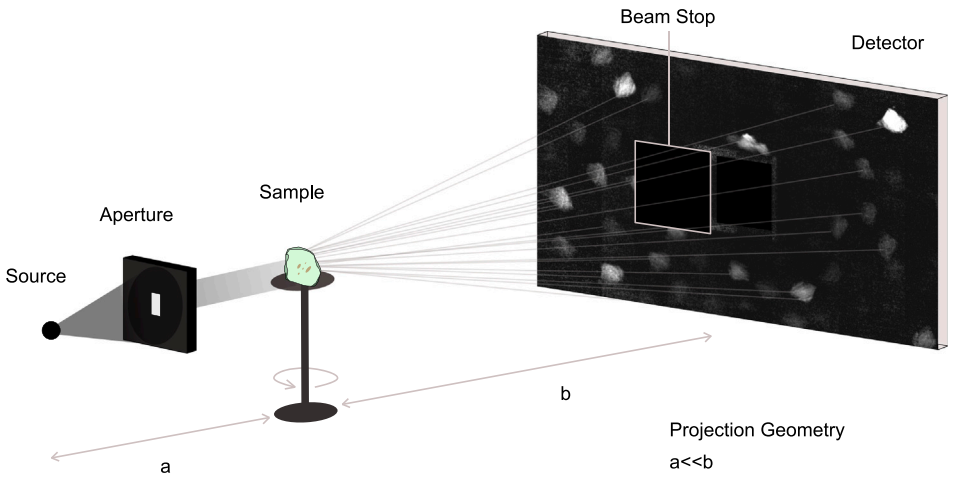

Fig. 1. Schematic diagram of the experimental setup for a LabDCT study.

from the surface, allowing for further EBSD analyses at various depths within the material. In this way, repeated milling and two-dimensional EBSD measurements (serial sectioning), enable high resolution three-dimensional microstructural characterisation. Although effective for small volumes, FIB serial sectioning is extremely time-consuming and generally only conducted on volumes of up to 50 × 50×50 μm (i.e. 125 000 μm^3), although plasma-FIB or femtosecond laser FIB instruments can allow for larger volume removal and analyses (Xu et al., 2007; West and Thomson, 2009). Consequently, this combination of techniques is generally unsuitable for investigating larger scale features, such as melt inclusion populations where sizes typically range from 10s to 100s μm, and their host crystals which can be >1 mm in size. In addition to size limitations, combined FIB sectioning and EBSD analysis is inherently destructive, which poses challenges for studies where subsequent analysis may be necessary, or where sample material is scarce and must be preserved.

Non-destructive, three-dimensional microstructural characterisation can be performed using synchrotron-based X-ray techniques. Several three-dimensional X-ray Diffraction (3DXRD) techniques have been developed, utilising high energy X-rays from synchrotron-based beams (monochromatic or polychromatic) (Larson et al., 2002; Ludwig et al., 2008; Poulsen, 2012; Chen et al., 2023). Synchrotron-based 3DXRD techniques are comprehensive and effective for microstructural investigation, allowing for the determination of crystal structure, orientation and strain tensors at the micrometre level (Larson et al., 2002; Ludwig et al., 2009). However, this analysis is significantly limited by the requirement for specialised equipment, technical expertise and the restrictions associated with gaining beam time and access to synchrotron facilities.

Diffraction Contrast Tomography (DCT) is a variant of 3DXRD that combines three-dimensional X-ray diffraction microscopy and image reconstruction from X-ray absorption contrast tomography (Ludwig et al., 2009). Over the last decade this technique has been adapted for use with a conventional laboratory X-ray microscope setup, providing the technique often referred to as laboratory-DCT (LabDCT) (Ludwig et al., 2008; King et al., 2013; McDonald et al., 2015; Holzner et al., 2016; Bachmann et al., 2019). X-ray diffraction patterns are combined with spatial and volumetric characterisation, obtained from X-ray micro-Computed Tomography (micro-CT), to generate three-dimensional grain maps of polycrystalline materials with crystallographic information.

Micro-CT utilises the penetrative power of X-rays to characterise the interior of a sample based on the X-ray attenuation contrast (a function of the material density and atomic number) (Withers et al., 2021). A sample is rotated within the path of an X-ray beam, with two-dimensional projections collected on a detector as the X-rays pass through the sample. Projections are collected as the sample rotates around 360°, and these are back-projected using computational algorithms to produce a three-dimensional model of the X-ray absorption contrast within the sample (Withers et al., 2021; Richard et al., 2019).

A DCT scan is acquired with a similar experimental setup to a micro-CT scan. An aperture and beam stop are added, and the accelerating voltage and projection parameters are selected to ensure diffraction spots are clearly separated in the acquired diffraction patterns, processed using dedicated DCT reconstruction software (King et al., 2013; Holzner et al., 2016; Bachmann et al., 2019). Diffraction patterns are generated by the interaction of X-rays and lattice planes within a crystalline sample when the Bragg condition is satisfied ($n\lambda = 2d \sin\theta$) (Ludwig et al., 2008). X-rays pass through the aperture, directed at the sample which is mounted on a rotating stage. A beam stop is positioned to intercept the incident X-ray beam, allowing only diffracted X-rays to be collected at the detector. The diffracted X-rays form an array of 'spots' in each projection, producing a distinctive diffraction pattern characteristic of the mineral, each grain and its crystallographic orientation. The sample is rotated around 360°, and projections are collected at angular increments throughout the scan (typically 180–300 projections per scan) (King et al., 2013). The resultant projections are noise-filtered and the spots are indexed by comparison with simulated diffraction patterns, selected from an extensive database of minerals and crystalline materials using specialist software (Niverty et al., 2019; Bachmann et al., 2019). The combination of micro-CT and DCT, adapted to a conventional and relatively accessible laboratory-scale X-ray microscope setup provides the opportunity for rapid, non-destructive microstructural characterisation of polycrystalline samples at the microscopic scale. A schematic of the instrumental configuration is shown in Fig. 1.

The development and implementation of LabDCT has grown predominantly within material sciences, focusing on metallic samples (McDonald et al., 2015; Holzner et al., 2016; Bachmann et al., 2019; Niverty et al., 2019). Despite its significant advantages over serial sectioning and EBSD, and the wider availability of suitable equipment compared with synchrotron-based 3DXRD, the use of LabDCT for natural materials and geological investigation remains limited, with only a handful of studies to date (Pankhurst et al., 2019; Andrew et al., 2019; Chen et al., 2023, 2024; Barbee et al., 2024, 2025; Pankhurst et al., 2025). In this study, we demonstrate the value that LabDCT can provide for investigating geological materials without the need for sample destruction. We apply this technique to explore olivine-hosted melt inclusion population characteristics and how they can be linked to host crystallography.

Inclusions are a common occurrence in natural and synthetic minerals, providing valuable insights into the geological history and formation conditions of their host crystals, as well as affecting physical

and material characteristics (Sorby, 1858; Roedder, 1979; Timms et al., 2012; Cannatelli et al., 2016; Campomenosi et al., 2024; Cadena et al., 2024; Arpa et al., 2025). Encapsulated during mineral growth, inclusions preserve a record of physical and chemical conditions at the time of host formation. Consequently, understanding entrapment mechanisms and physicochemical controls on inclusion characteristics and spatial arrangement is essential for refining interpretations of these features, as well as advancing knowledge of mineral growth processes and the physical behaviour of inclusion-bearing materials (Timms et al., 2012; Campomenosi et al., 2024; Arpa et al., 2025). Techniques such as single-crystal X-ray diffraction have been applied to investigate mineral inclusion crystallography, predominantly within diamond hosts (Milani et al., 2016; Nimis et al., 2019; Angel et al., 2022). However, the combination of LabDCT and micro-CT to provide crystallographic context and develop a three-dimensional model of internal crystal structures and inclusion populations is a new advance for laboratory-based X-ray microscopy.

This study targets melt inclusions, small pockets of quenched melt trapped within volcanic olivine crystals (Roedder, 1979; Cannatelli et al., 2016; Danyushevsky et al., 2002; Sobolev, 1996). Melt inclusion entrapment is hypothesised to occur as the result of irregularities in crystal growth conditions, such as rapid skeletal or dendritic growth, or through the attachment of an immiscible phase to the growing crystal edge. Secondary processes, such as dissolution and crystal regrowth, and cracking and resealing, can also produce secondary inclusions (Roedder, 1979; Wallace et al., 2021). Because the host crystal chemically isolates the inclusion, melt compositions that might otherwise be altered by fractionation, crystallisation, or mixing processes are preserved, along with magmatic volatiles that would typically be lost during degassing (Lowenstern et al., 1995; Moore et al., 2015; Wallace et al., 2021; Sobolev and Chaussidon, 1996). Melt inclusions are therefore significant for understanding magmatic systems and processes, and have been the object of significant analytical and geochemical investigation for multiple decades (Roedder, 1979; Lowenstern et al., 1995; Cannatelli et al., 2016; Wallace et al., 2021). Understanding the mechanisms controlling the entrapment of melt inclusions is significant for the correct petrological interpretation of the data and insights they can provide (Roedder, 1979; Lowenstern et al., 1995; Faure and Schiano, 2005; Arpa et al., 2025).

Olivine ($(Mg,Fe)_2SiO_4$), is an orthorhombic mineral that dominates the earth's upper mantle and plays a central role in the petrogenesis of basaltic melts. It crystallises early in olivine-saturated magmas, making it a common constituent of volcanic products, magmatic rocks, and also typically forms part of meteorites (Wallace et al., 2021; Welsch et al., 2023b). Due to its early crystallisation and prevalence in a wide range of magma compositions, olivine is often used to understand a multitude of magmatic processes, and in particular is targeted for melt inclusion studies (Cannatelli et al., 2016; Wallace et al., 2021; Welsch et al., 2023b). Olivine is one of the only natural minerals that has been resolved using LabDCT, with successful determination of the crystallographic orientation of crystal shards and subgrains (Pankhurst et al., 2019, 2025).

Features such as morphology, population characteristics and spatial arrangement, are usually used to infer the nature of melt inclusions (primary or secondary), and therefore their entrapment mechanism. These observations are often qualitative, limited by inclusion visibility when considering three-dimensional characteristics, or restricted to two-dimensional interpretations after destructive sample preparation involving the intersection and removal of crystal material to expose inclusions at the sample surface. Three-dimensional investigations are now more common, enabled by the adoption of micro-CT into melt inclusion studies, significantly improving the understanding of inclusion geometry, population characteristics, shape, and volume quantification (Pamukcu et al., 2013, 2015; Créon et al., 2018; Richard et al., 2019; Hanyu et al., 2020; van Gerve et al., 2024; Jorgenson et al., 2025). While useful and effective, micro-CT is still not a commonly applied technique in the typical melt inclusion analytical workflow.

Preferential alignment of melt inclusion populations within olivine crystals is a characteristic that has been noted from both optical observations, and via micro-CT (Faure and Schiano, 2005; Metrich and Wallace, 2008; Thornhill et al., 2026). Although sometimes observed, there has been little investigation into the cause or significance of this feature and its occurrence in natural magmatic olivine crystals. Where identified, it has generally not been possible to discern whether alignment is related to host crystallographic features due to irregular crystal shapes, glass films coating the crystals, or fractured surfaces obscuring crystal habit.

In this study, we apply a combination of micro-CT and LabDCT to investigate whether inclusion orientation can be linked to the host olivine crystallography, and what this may imply for the magmatic conditions during inclusion entrapment. The method developed in this investigation allows for comparison between inclusion orientation, determined through micro-CT processing and analysis, and crystal orientation determined from LabDCT. This could be transferable to any mineral and melt inclusion system that can be scanned with micro-CT and resolved with LabDCT. Provided the X-ray absorption contrast is sufficient to segment the internal phases, features such as fluid, void space or melt inclusions can be investigated. With modification, this method would also be suitable for producing pole figures for comparison of mineral inclusion orientations within their crystalline host. This provides a valuable, non-destructive, three-dimensional insight into mineral and inclusion systems and entrapment processes, significantly contributing to inclusion studies and the understanding of mineral growth regimes.

2. Materials and methods

2.1. Sample preparation

Olivine crystals analysed in this study were collected from the eruptive deposits of Mocho Choshuenco, a large volcanic complex in Southern Chile (Rawson et al., 2015). Loose olivine crystals were hand picked under a binocular microscope from volcanic scoria deposits from multiple different eruption units. Over 100 grains were picked that contained visible internal melt inclusion features. These were scanned using a conventional micro-CT set-up at the University of Leeds (Zeiss Versa XRM 400), for melt inclusion characterisation, and volume quantification. Crystals exhibiting melt inclusion populations that appeared to be visibly aligned were separated for further investigation. In total, six crystals with visibly aligned melt inclusions, and two with randomly oriented inclusions, were selected for analysis with LabDCT.

Selected crystals were mounted on the inside of an X-ray transparent tube (plastic straw) with a diameter of ca. 3 mm using double-sided tape. The position of crystals was staggered vertically to enable individual scanning using the Helical Phyllotaxis scan mode of the machine. The straw was re-rolled and secured with tape, then positioned in the micro-CT scanner on a rotating sample holder.

2.2. Sample measurements

Olivine crystals were scanned using a Zeiss Xradia Crystal CT instrument, located at the Hercules Facility in the College of Science and Engineering at the University of Leicester, UK. Scans were performed using the Zeiss 'Scout and Scan' software (version 16.1). For each crystal, two types of scans were collected : (1) an initial absorption contrast micro-CT, followed by (2) a DCT scan of the same region. Individual scans ranged from ca. 1 to 1.5 h in duration. Full scan conditions and analytical parameters for both scan types are provided in Tables 1 and 2.

Table 1
Micro-CT scan parameters.

Parameter	Value
Voltage	80 kV
Power	7 W
Current	87 µA
Filter	None
Source to Sample	20 mm
Sample to Detector	300 mm
Detector	CMOS Flat Panel (3072 × 1944 pixels)
Geometric Magnification	Approx. 16×
Pixel Size	4.24 µm to 4.67 µm
No. Projections	601 to 801
Exposure Time	0.3 s (per frame)
Frames per projection	3

Table 2
DCT scan parameters.

Parameter	Value
Voltage	80 kV
Power	7 W
Current	87 µA
Aperture	750 µm × 750 µm
Beam Stop	45 mm × 45 mm
Source to Sample	20 mm
Sample to Detector	300 mm
Detector	CMOS Flat Panel (3072 × 1944 pixels)
Geometric Magnification	Approx. 16×
Detector Binning	2
Projections	221 (per rotation)
Exposure Time	15 s (per frame)
Frames per projection	3

2.3. Data reconstruction and reduction

LabDCT scan reconstructions were performed using the GrainMapper3D software (version 4.0), developed by XNovo Technology. Absorption data from the initial micro-CT scan were used to define a 'space envelope' corresponding to each olivine crystal, which constrained the volume for subsequent DCT pattern reconstruction. The samples consisted predominantly of singular olivine grains, allowing for straightforward analysis using a simple processing workflow that largely followed the default processing recommendations within the software package.

A standard segmentation was applied to the DCT projections to produce binary images of the diffraction spots. These were compared with forward simulations of predicted diffraction patterns, generated within the software for the mineral specified (olivine). The composition of olivine crystals in this study was not determined prior to these scans, so a pure forsterite composition was used (Mg_2SiO_4). If necessary, data analysis could be subsequently refined with a known olivine composition. However, the compositional differences between the two olivine end members, forsterite and fayalite (Fe_2SiO_4) have little effect on the lattice parameters and unit cell, and therefore it is likely that the composition would not significantly affect the outcome of this study. The 'goodness of fit' for computed diffraction pattern simulations is quantified with the 'completeness' parameter:

$$\text{Completeness} = \frac{\text{Spots on detector}}{\text{Simulated spots}} \quad (1)$$

In general, completeness values exceeding 85% are considered reliable for DCT solutions, with 45% typically regarded as the minimum acceptable value (Bachmann et al., 2019). Due to the simplicity of the samples analysed, each containing just a single olivine crystal, the completeness values for all LabDCT scans in this study were above 90%. As a result, iterative refinement of solutions was unnecessary. The LabDCT processing yielded the crystallographic orientation of each olivine within the scan space, with crystal axes extracted from the DCT dataset as Euler angles in Bunge notation.

Table 3
DCT reconstruction parameters.

Parameter	Value
Voxel Size	5 µm
Minimum Completeness	45 %
Completeness Cut Off	0 %
Trust Completeness	85 %
Completeness Drop Off	2 %
Boosting	95 %
Misorientation Threshold	0.5°
Crystal Structure Name	Olivine (forsterite: Mg_2SiO_4)
Crystal System	Orthorhombic (mmm)
Space Group	62
Unit Cell Dimensions	a = 4.779 Å, b = 10.277 Å, c = 5.995 Å α = 90°, β = 90°, γ = 90°
Reflections	{0 0 4}, {0 6 2}, {2 2 2}, {1 3 0} {2 4 0}, {4 0 0}, {1 1 2}

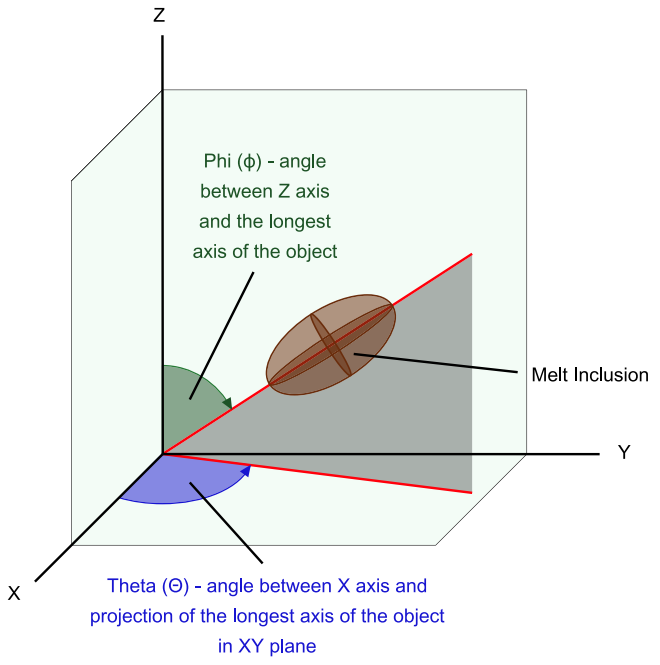

Fig. 2. Schematic diagram defining the Phi (ϕ) and Theta (θ) angles generated in Dragonfly Pro for the description of inclusion orientation within the sample reference frame.

The reconstruction parameters, and crystallographic data used to process the LabDCT scans in GrainMapper3D are provided in Table 3.

2.4. Data processing

Additional processing was required to produce the data necessary to compare the DCT-derived crystallographic orientation of the olivine hosts with the morphology of their melt inclusions.

Melt inclusion orientations and morphological characteristics were generated from the absorption contrast data obtained from the micro-CT scans for each crystal. To analyse this, data were loaded into ORS Dragonfly Pro (version 2022.2), an X-ray image visualisation and analysis software. To enable direct comparison with LabDCT outputs processed in GrainMapper3D, an axis transformation was applied to the micro-CT data. Using the 'Legacy Mode' function in Dragonfly Pro, the acquisition axes were converted from the micro-CT default ('XYZ') to the DCT convention ('XZY'), ensuring consistency and comparability between the two datasets.

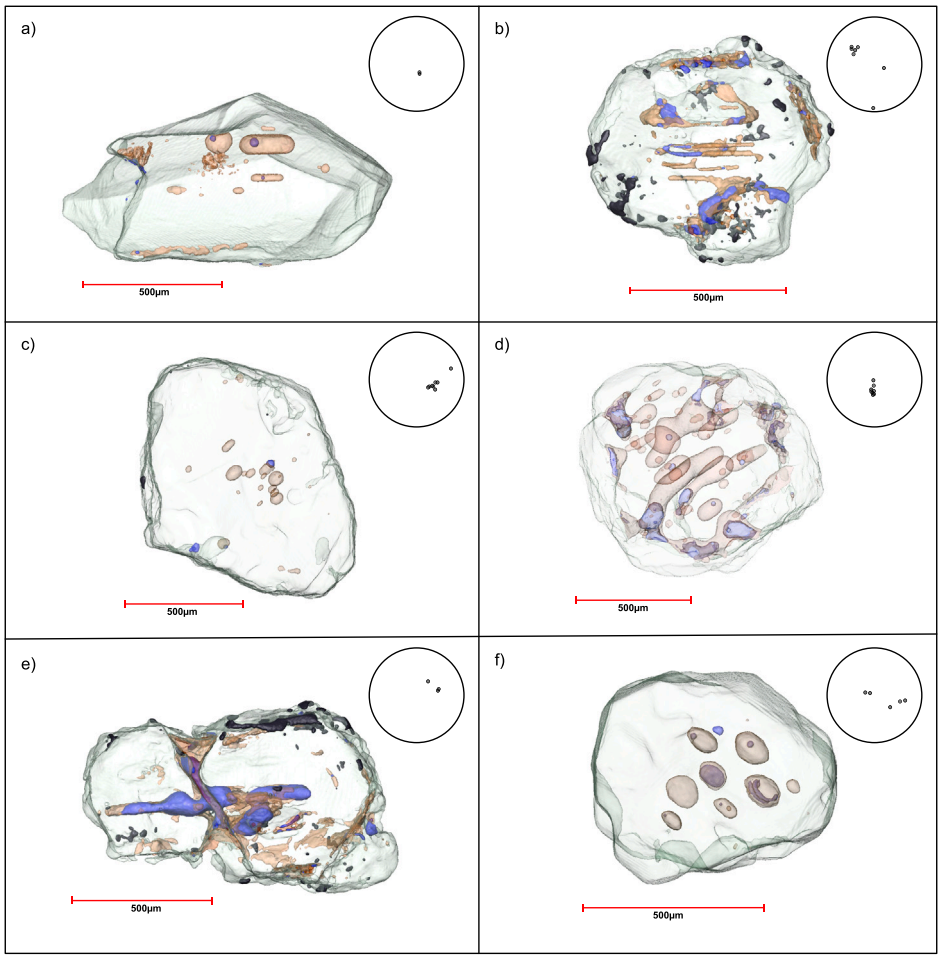

Fig. 3. micro-CT reconstructions of olivine crystals scanned in this study (green — olivine crystal, brown — melt inclusion glass, blue — bubble/void space, black — spinel). Pole figures for the orientation of the long axis of melt inclusions are also included at the top right of each reconstruction. Clustering clearly indicates a common orientation, however these are relative to the scan reference frame and contain no crystallographic context.

Melt inclusions within each olivine crystal were manually thresholded and segmented using two-dimensional slices. Greyscale intensity ranges within the projections were visually checked to ensure segmentation accurately captured all the relevant internal inclusion phases and host crystal. This segmentation produced a new object within the Dragonfly software interface, which was converted to dataset where each inclusion can be analysed individually as a separate feature. Analysis of the inclusion dataset was conducted using the 'Compute Measurements' function. This generated a list of morphological characteristics and measurements, including the orientation, for each segmented melt inclusion within the crystal. Inclusion orientation is represented in the software using Theta (θ) and Phi (ϕ) values for the long axes of the melt inclusions. These are defined as the angle between the X axis and the projection of the longest axis of the melt inclusion in the XY plane, and the angle between the Z axis and the longest axis of the melt inclusion, respectively. These parameters are also visually defined in Fig. 2.

To compare the DCT-derived crystallographic orientation data from the host olivine grains with the inclusions' morphology and spatial orientation data obtained from micro-CT, it was necessary to combine these two types of information in a single display with a common reference frame. The approach adopted in this study involved calculating the crystallographic direction parallel to the long axis of each inclusion, and then plotting this information on an inverse pole figure (IPF). This made it straightforward to identify any dominant crystallographic relationship between the inclusion morphology and the host olivine crystallography, with a single inverse pole figure displaying all the inclusions in each olivine grain. No single commercially available software has been designed for this data manipulation.

Here we used the following steps, combining three separate software tools: (1) The inclusion orientations were calculated in Dragonfly Pro, using the micro-CT data as previously described, yielding Theta and Phi values for the inclusion long axes. (2) A file containing the relevant crystallographic orientation for the host olivine via labDCT was produced. In this study we used AZtecCrystal, an EBSD data processing software, which requires a Hierarchical Data Format (HDF) file type. The HDF files were generated for this study using the free software, HDFView (downloadable from the HDFGroup website - https://www.hdfgroup.org/download-hdfview/). The crystallographic orientation data were inputted into these files as Euler angles, using the Bunge notation. (3) This host-crystal file was opened in AZtecCrystal (version 3.2, from Oxford Instruments). The Theta and Phi values for each inclusion were used to transform the sample coordinate system (CS0) to align the inclusion long axis with the Z0 direction. (4) An IPF (relative to the Z0 direction) was plotted to show the inclusion orientation relative to the crystal orientation of the host grain. Steps (3) and (4) were repeated for each inclusion within the same olivine grain. The individual IPFs were then combined into a single plot for each olivine, showing the orientation of the long axis of each melt inclusion with reference to the host olivine crystallography. The method described above provides a general framework that can be adapted and

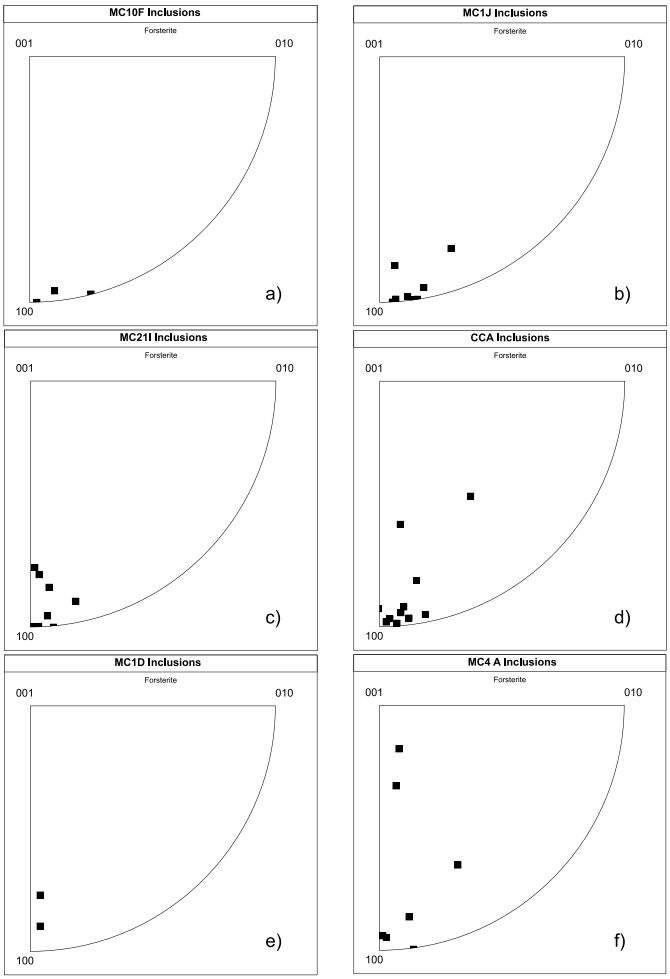

Fig. 4. Inverse pole figures generated for each olivine crystal and the inclusions within (labels correlate with the crystals in Fig. 3). The orientation of the long axis of inclusions is compared to the crystallography of the olivine host. Clusters of points around the [100] direction correspond to an alignment with the *a*-axis of the host olivines. Spread in data may reflect inconsistency in orientation determination due to the low aspect ratio of inclusions (particularly pertinent in (f) where inclusions are generally more rounded).

applied to compare the orientation of internal phases such as inclusions with their mineral host using LabDCT.

3. Results

All olivine crystals were successfully scanned and reconstructed. Orientation Phi and Theta angles, generated from the processed micro-CT data for each segmented melt inclusion revealed a clear common alignment of inclusion populations within individual crystals. This can be visually confirmed from three-dimensional reconstructions produced from the micro-CT data. Similarly, pole figures of the Phi and Theta angles for melt inclusion orientation show shared alignment, with the orientation of the long axes clustering together (see Fig. 3). These plots contain no crystallographic context, and the shape of the olivine crystals in this study do not allow the determination of the host olivine crystallographic orientation, highlighting the necessity for DCT data to determine the crystallographic relationship between inclusions and their host mineral.

When combined with DCT data and plotted on IPFs referenced to the host olivine crystallography, these inclusion orientations predominantly cluster around the *a*-axis ([100]) (Fig. 4). Some scatter is observed, likely reflecting variable inclusion morphology. For example, the aspect ratio of inclusions can strongly affect the accuracy of determining inclusion orientation, with greater uncertainties for more equant inclusions. This is observed in the scatter seen in the pole figures for f) in Figs. 3 and 4, the result of rounded melt inclusion geometries with low aspect ratios relative to the other crystals in the study. Melt inclusion size and morphology varied significantly between crystals. All inclusions considered in this study were large enough (> 50 μm in length) to be resolvable at the micro-CT scan resolution used (pixel dimension ca. 4.5 μm) (Richard et al., 2019). Any inclusions smaller than > 50 μm in length were not considered due to the uncertainty associated with segmentation and orientation determination.

For contrast, two olivine crystals containing randomly oriented melt inclusions were also scanned and analysed under the same conditions and processing procedure. These inclusions display no visible alignment, and there is also no evidence for crystallographic control of inclusion orientation (Fig. 5). The morphology of inclusions in these crystals is generally more rounded, and inclusions are scattered within the host crystal rather than near the centre, as seen in the majority of crystals in Fig. 3.

4. Discussion

Melt inclusions with preferred orientations have been previously documented in olivine, often visible in optical images (Faure and Schiano, 2005; Metrich and Wallace, 2008; Welsch et al., 2013; Steele-MacInnis et al., 2017; Salas et al., 2021; Thornhill et al., 2026). Alignment of primary inclusions has been proposed to reflect the growth regime of the host olivine; however, there has been little targeted research to support this hypothesis. This study provides the first three-dimensional evidence for melt inclusion alignment in natural magmatic olivine crystals. The results also confirm a crystallographic control on this orientation, with inclusions consistently aligned with the *a*-axis of their host crystal. This implies that inclusion entrapment, in some cases, may be governed by the growth mechanics of the olivine (i.e. dendritic, skeletal, disequilibrium). However, visible alignment is not ubiquitous with all olivine-hosted inclusion populations and it should be noted that, due to the resolution constraints of the technique used, only inclusions larger than around 30 μm are considered in this study.

The principal growth direction of natural olivine is thought to be sensitive to undercooling within the magmatic system, with high undercooling resulting in skeletal and dendritic habits that form due to rapid crystallisation under thermal disequilibrium (Faure and Schiano, 2005; Mourey and Shea, 2019; Salas et al., 2021; Welsch et al., 2023a). Three-dimensional experimental observations demonstrate that rapid olivine growth along the *a*-axis occurs under moderate to high degrees of undercooling ($-\Delta T$ = 40 °C to 60 °C (Mourey and Shea, 2019)). Similarly, swallowtail olivine crystals, the product of rapid crystallisation, have been shown to form cavities that align with the a-axis (Faure and Schiano, 2005). Two-dimensional observations of these experimentally grown swallowtail olivines, subject to several heating and cooling cycles, show preferentially aligned melt inclusions, elongated along the *a*-axis of the host crystal (Faure and Schiano, 2005). Our findings support these experimental observations, providing the first three-dimensional evidence of the occurrence of aligned melt inclusions within natural olivine crystals, consistently orientated along the *a*-axis. A schematic diagram suggesting the process for a-aligned melt inclusion populations is provided in Fig. 6.

Dendritic olivine, and inclusions with elongated *a*-axis morphologies, have been proven to form experimentally through thermal disequilibrium events, however evidence of this phenomena in natural magmatic olivines is rarer (Faure and Schiano, 2005; Mourey and Shea, 2019). The conditions required are analogous to natural magmatic processes such as magma mixing and cyclical convection, interaction of

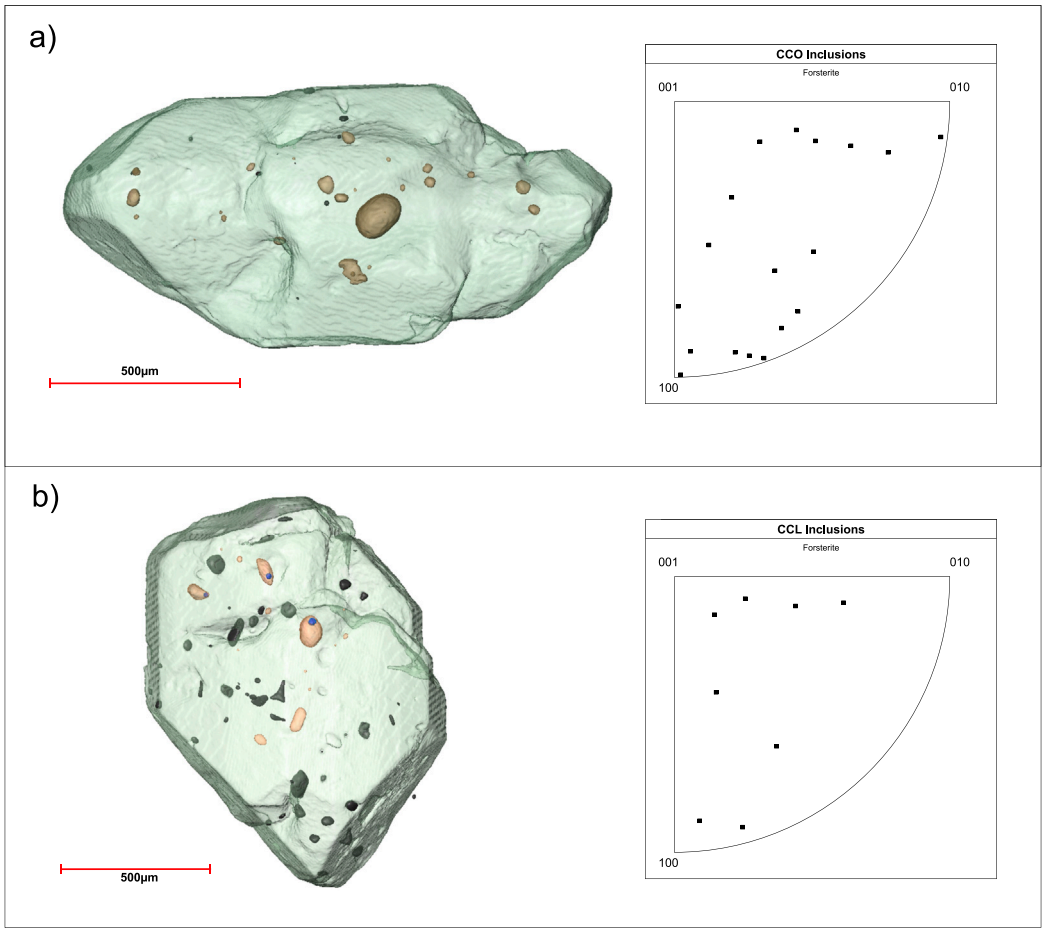

Fig. 5. (a) and (b) micro-CT reconstructions of two scanned crystals containing inclusions with no visible alignment, and IPF figures generated using the method outlined in this study. The IPFs show a significant scatter in orientation, with no clear relationship between the host olivine crystallography and the inclusion populations.

magma with cool crust and decompression-driven degassing. These processes are common in active volcanic systems, such as the volcano that crystals from this study were sourced from. The Mocho-Choshuenco volcanic system has been particularly active over the last 10 thousand years, likely the result of multiple magmatic processes and recharge events, with the olivines in this study selected from a range of different eruption deposits spanning this time period (Rawson et al., 2015).

Melt inclusion morphology can also be affected by post entrapment modification processes such as melt crystallisation, bubble formation, and faceting (Créon et al., 2018; Rasmussen et al., 2020; Wallace et al., 2021; Pamukcu et al., 2015). Although no crystallisation features were visible in the micro-CT projections and 3D renders, it is possible that fine scale crystallisation may not be visible at the resolution used here (pixel size ca. 4.5 µm). Regardless, it is unlikely that this mechanism could be responsible for inclusion alignment. Faceting, in which inclusions adopt negative crystal shapes which reflect their host crystal habit, is a secondary feature that reflects post entrapment maturation of inclusion morphology to minimise surface energy. This is more commonly observed in quartz-hosted melt inclusions, however there are also occurrences of olivine-hosted inclusion faceting documented in a handful studies (Schiano, 2003; Pamukcu et al., 2015; Wallace et al., 2021). While it is plausible that faceting may result in a more uniform population of inclusions that could replicate the crystallographic axes of their host and therefore show alignment, the large aspect ratios of inclusions within this study and lack of evidence for faceting seen in the micro-CT reconstructions makes this unlikely.

To comprehensively discern the processes responsible for inclusion alignment with host crystallography, further geochemical investigation is needed. Trace element mapping in olivine may be a good solution to determine if rapid, initial dendritic growth has occurred in these crystals. Distinctive zoning patterns of slow-diffusing elements in olivine (i.e. Phosphorous and Aluminium), have been observed in both experimental and natural olivine crystals, reflecting a dendritic pattern that has been associated with rapid skeletal crystal growth and the subsequent incorporation of incompatible trace elements in early-formed branches (Welsch et al., 2013; Xing et al., 2017; Shea et al., 2019; First et al., 2020; Xing et al., 2022; Welsch et al., 2023a). If trace element zoning is present in the crystals from this study, this would support the hypothesis that inclusion alignment is a growth feature, reflecting an initial period of accelerated olivine growth along the *a*-axis, likely due to undercooling and magmatic processes.

5. Outlook and applications

Importantly, the DCT data collected in this study allows for targeted further analyses, and facilitates the development of testable scientific hypotheses prior to destructive sample preparation and analytical techniques. The crystallographic orientation of each olivine, along with the absorption contrast data and three-dimensional reconstructions, allow for precise sample preparation such as determining the optimum plane for intersection prior to geochemical analyses. Sample intersection using techniques such as plasma-FIB or femtosecond laser FIB are a logical progression from the analyses in this study, and even intersection by hand-polishing would be significantly improved if these techniques are not available. For the crystals in this study, research is ongoing, using a combination of correlative femtosecond laser sectioning with broad

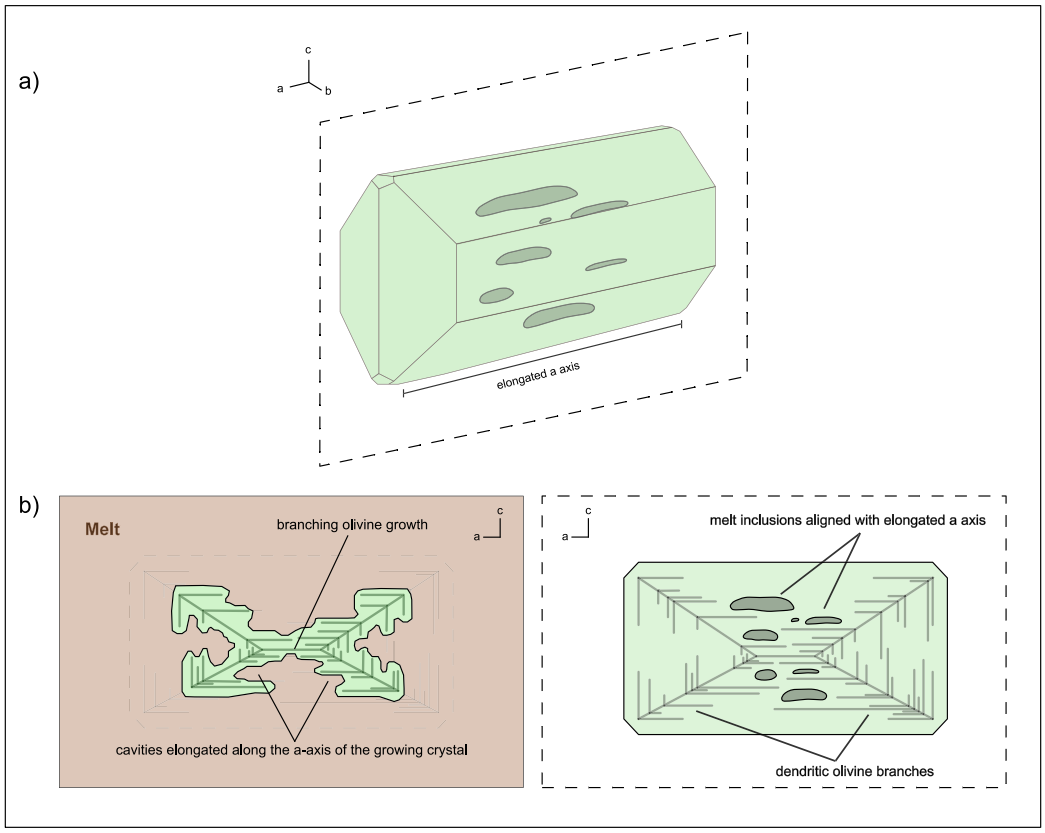

Fig. 6. (a) Schematic of typical olivine crystal habit with an elongated *a*-axis, the result of growth associated with moderate to high undercooling. Dashed rectangle shows the cross-section plane for the schematic below. (b) Schematic diagram showing a branched olivine crystal core. These branches may be enriched in trace elements such as phosphorus and aluminium. The initial skeletal network provides a framework for the entrapment of preferentially aligned melt inclusions, oriented parallel to the elongated *a*-axis. Slower growth and 'ripening' results in the polyhedral crystal habit, and the encapsulation of aligned melt inclusions.

ion beam (BIB) polishing to produce cross sections through the olivine grains. These sections are intentionally aligned perpendicular to the inclusions' long axes (i.e. parallel with the host olivine's (100) plane) and enable high resolution EBSD analyses for the characterisation of deformation and strain effects associated with the inclusions' formation. This is being followed by trace element mapping of phosphorus and aluminium using Electron Probe Micro-Analysis (EPMA) to further investigate and confirm the geochemical mechanisms associated with the inclusion alignment. These results will be published in a subsequent manuscript.

The use of these non-destructive, three-dimensional analytical techniques provides an effective screening tool for crystal or sample populations. Important features such as sample integrity (e.g. presence of cracks) and complexity, phase identification, crystallography, and inclusion morphology and population characteristics can all be determined rapidly, significantly streamlining further analytical procedures and sample preparation. As highlighted in this study, the three-dimensional characterisation of the spatial distribution of inclusions within materials, and their relationship to host crystallography, is important for understanding features such as entrapment mechanisms, mineral growth regimes and kinetics. This can also be significant for constraining mechanical properties of inclusion-bearing minerals. Inclusions have been found to cause localised crystal plasticity and enhanced diffusion pathways, along with concentrating strain and controlling the nucleation of brittle failure within minerals (Timms et al., 2012; Cadena et al., 2024). Understanding inclusion population characteristics such as morphology, spatial arrangement, and controls such as crystallographic alignment are therefore significant for better understanding the behaviour of materials under changing physical conditions, as well as deciphering the conditions of their formation.

LabDCT and micro-CT are evolving analytical techniques, however their potential scientific significance is evident. The wider availability of this technique in X-ray microscopy laboratories opens up opportunities for more scientists to analyse materials and microstructures in three-dimensions, with meaningful sample volumes of up to 8 mm^3 (Holzner et al., 2016). The non-destructive nature also provides the capability to facilitate '4D' studies, where microstructural evolution can be tracked over time during repeated observations. This is particularly significant for understanding how materials, both natural and synthetic, behave under varying physical and chemical conditions (Sun et al., 2024).

There are, however, limitations associated with this method. Unlike other 3DXRD techniques, strained crystals cannot be easily analysed, as lattice distortion is not resolvable with the current algorithms and software. There are also grain size limitations, with grains needing to be large enough to be resolvable (e.g. typically diameters >30 μm). Difficulties can also arise if grain sizes approach that of the aperture used during scanning. For singular grains such as this study, the limited number of spots per projection means that this is manageable, however for samples consisting of multiple larger grains (typically >250 μm), difficulties can arise in separating and indexing the patterns and diffraction spots.

For multiphase materials with resolvable grain sizes, correlative studies between EBSD and LabDCT show good agreement for features such as centre-of-mass position, orientation, and grain size and shape of phases present, highlighting the utility and validity of this technique when applied to the right sample (Ball et al., 2023; Chen et al., 2023). Therefore, for simple features such as the single crystals and melt inclusions considered in this study, the technique is more than sufficient. It would also be possible to apply a modified version of

this method to consider the orientation of crystalline phases included within a host grain, provided they are within the typical resolvable size ranges for the technique. Evidently, for a large number of material and geoscience studies, LabDCT has the capability to generate insightful and pertinent, three-dimensional data.

6. Conclusions

The method described in this paper provides a framework for processing micro-CT and LabDCT derived data to investigate the relationship between inclusions and their mineral host. We successfully apply these techniques to populations of preferentially aligned melt inclusions hosted in magmatic olivine crystals. The results show that these inclusions consistently align with the *a*-axis of their olivine hosts, suggesting a possible crystallographic control during inclusion entrapment. This alignment may indicate the occurrence of rapid olivine growth due to undercooling in the magmatic system, however further investigation would be required to confirm this. This method is not limited to the exclusive investigation of olivine crystals and their melt inclusions. Any mineral that can be processed by LabDCT can be investigated, and internal features of interest may include melt, fluid or mineral inclusions. The only requirement is that internal features need sufficient attenuation contrast for micro-CT investigation and segmentation, and the sample or object of interest must lack internal strain and have resolvable grain sizes for LabDCT analysis.

This study aims to highlight the value of using X-ray microscopy techniques for investigating natural materials and processes. Micro-CT and LabDCT are complimentary techniques that allow for non-destructive, three-dimensional imaging and the characterisation of natural and synthetic materials and their microstructure. For studies such as melt inclusion analyses, these techniques provide a valuable scientific insight without the need for sample destruction, allowing for the development and investigation of new areas of research. This is significant for understanding processes such as inclusion entrapment mechanisms and mineral growth regimes and kinetics, along with understanding mechanical and physical properties of inclusion-bearing minerals. LabDCT and micro-CT provide the opportunity to obtain insightful and pertinent, three-dimensional data and crystallographic information for polyphase materials, an opportunity that is currently under-utilised in geological sciences.

CRediT authorship contribution statement

Helen Thornhill: Writing – review & editing, Writing – original draft, Visualization, Validation, Resources, Project administration, Methodology, Investigation, Funding acquisition, Formal analysis, Data curation, Conceptualization. **Patrick Trimby:** Writing – review & editing, Visualization, Validation, Software, Resources, Methodology, Investigation, Funding acquisition, Formal analysis, Data curation, Conceptualization. **Gareth Douglas:** Writing – review & editing, Visualization, Software, Resources, Methodology, Investigation, Formal analysis, Data curation. **Alice Macente:** Writing – review & editing, Supervision, Software, Methodology, Investigation, Data curation. **David Ferguson:** Writing – review & editing, Supervision, Project administration. **Felix Boschetty:** Writing – review & editing, Supervision, Investigation.

Declaration of competing interest

The authors declare that they have no known competing financial interests or personal relationships that could have appeared to influence the work reported in this paper.

Acknowledgements

DCT imaging was performed at the Hercules Facility at the University of Leicester, supported by EPSRC, United Kingdom grant EP/X014614/1. The Hercules Facility is part of the ZEISS Labs@Location institute at the University of Leicester. Preliminary micro-CT imaging was conducted at the University of Leeds with the help of Alice Macente. This work was conducted as part of a project funded by the NERC Panorama DTP Programme, University of Leeds - Earth and Environment, Grant Reference Number: NE/S007458/1.

Data availability

Data will be made available on request.

References

Andrew, M., Bale, H., Gueninchault, N., Sun, J., Hanna, R., Maisano, J., Ketcham, R., Pankhurst, M., Zolensky, M., 2019. Non-invasive 3D crystallography of geological media in the laboratory. Microsc. Microanal. 25 (S2), 2460–2461.

Angel, R.J., Alvaro, M., Nestola, F., 2022. Crystallographic methods for non-destructive characterization of mineral inclusions in diamonds. Rev. Miner. Geochem. 88 (1), 257–305.

Arpa, M.C., Christenson, B., Zellmer, G.F., 2025. Melt inclusions from autocrysts and xenocrysts: considering crystal origin in interpreting volatile content and magmatic processes. Bull. Volcanol. 87 (9), 1–27.

Bachmann, F., Bale, H., Gueninchault, N., Holzner, C., Lauridsen, E.M., 2019. 3D grain reconstruction from laboratory diffraction contrast tomography. Appl. Crystallogr. 52 (3), 643–651.

Ball, J.A.D., Oddershede, J., Davis, C., Slater, C., Said, M., Vashishtha, H., Michalik, S., Collins, D.M., 2023. Registration between DCT and EBSD datasets for multiphase microstructures. Mater. Charact. 204, 113228.

Barbee, O., Oddershede, J., Purushottam Raj Purohit, R.R.P., Ånes, H., Engqvist, J., Svensson, A., Rathmann, N., Blunier, T., Bachmann, F., Hall, S., 2025. Mapping textures of polar ice cores using 3D laboratory X-ray microscopy. EarthArXiv Eprints X52Q89.

Barbee, O., Pankhurst, M., Bachmann, F., Oddershede, J., Sun, J., 2024. A sinusoidal twin boundary harmonizes with the elastic anisotropy of quartz. Res. Sq. - PrePrint.

Cadena, T., Manga, M., Befus, K., Tamura, N., 2024. Stressful crystal histories recorded around melt inclusions in volcanic quartz. Contrib. Miner. Pet. 179 (6), 60.

Campomenosi, N., Angel, R.J., Mihailova, B., Alvaro, M., 2024. Mineral host inclusion systems are a window into the solid-state rheology of the earth. Commun. Earth Environ. 5 (1), 660.

Cannatelli, C., Doherty, A.L., Esposito, R., Lima, A., De Vivo, B., 2016. Understanding a volcano through a droplet: A melt inclusion approach. J. Geochem. Explor. 171, 4–19.

Chen, X., Godel, B., Verrall, M., 2023. Comparison of laboratory diffraction contrast tomography and electron backscatter diffraction results: Application to naturally occurring chromites. Microsc. Microanal. 29 (6), 1901–1920.

Chen, X., Godel, B., Verrall, M., 2024. Postprocessing workflow for laboratory diffraction contrast tomography: A case study on chromite geomaterials. Microsc. Microanal. 30 (3), 440–455.

Créon, L., Levresse, G., Remusat, L., Bureau, H., Carrasco-Núñez, G., 2018. New method for initial composition determination of crystallized silicate melt inclusions. Chem. Geol. 483, 162–173.

Danyushevsky, L.V., McNeill, A.W., Sobolev, A.V., 2002. Experimental and petrological studies of melt inclusions in phenocrysts from mantle-derived magmas: an overview of techniques, advantages and complications. Chem. Geol. 183 (1–4), 5–24.

Faure, F., Schiano, P., 2005. Experimental investigation of equilibration conditions during forsterite growth and melt inclusion formation. Earth Planet. Sci. Lett. 236 (3–4), 882–898.

First, E.C., Leonhardi, T.C., Hammer, J.E., 2020. Effects of superheating magnitude on olivine growth. Contrib. Miner. Pet. 175 (2), 13.

van Gerve, T.D., Neave, D.A., Wieser, P., Lamadrid, H., Hulsbosch, N., Namur, O., 2024. The origin and differentiation of CO 2-rich primary melts in ocean island volcanoes: Integrating 3D X-Ray tomography with chemical microanalysis of olivine-hosted melt inclusions from pico (azores).. J. Petrol. 65 (2), egae006.

Hanyu, T., Yamamoto, J., Kimoto, K., Shimizu, K., Ushikubo, T., 2020. Determination of total CO2 in melt inclusions with shrinkage bubbles. Chem. Geol. 557, 119855.

Holzner, C., Lavery, L., Bale, H., Merkle, A., Mcdonald, S., Withers, P., Zhang, Y., Jensen, D.J., Kimura, M., Lyckegaard, A., et al., 2016. Diffraction contrast tomography in the laboratory–applications and future directions. Microsc. Today 24 (4), 34–43.

Humphreys, F.J., 2004. Characterisation of fine-scale microstructures by electron backscatter diffraction (EBSD). Scr. Mater. 51 (8), 771–776.

Jorgenson, C., Stuckelberger, M.E., Fevola, G., Falkenberg, G., Kaiser, T., Wilde, F., Weber, G., Giordano, G., Caricchi, L., 2025. A myriad of melt inclusions: A 3D analysis of melt inclusions reveals the gas-rich Magma reservoir of Colli Albani Volcano (Italy). J. Petrol. 66 (3), egaf012.

Kahl, W.A., Dilissen, N., Hidas, K., Garrido, C.J., López-Sánchez-vizcaíno, V., Romńn-Alpiste, M.J., 2017. 3-d microstructure of olivine in complex geological materials reconstructed by correlative X-ray-CT and EBSD analyses. J. Microsc. 268 (2), 193–207.

King, A., Reischig, P., Adrien, J., Ludwig, W., 2013. First laboratory X-ray diffraction contrast tomography for grain mapping of polycrystals. Appl. Crystallogr. 46 (6), 1734–1740.

Larson, B.C., Yang, W., Ice, G.E., Budai, J.D., Tischler, J.Z., 2002. Three-dimensional X-ray structural microscopy with submicrometre resolution. Nature 415 (6874), 887–890.

Lowenstern, J.B., Thompson, J.F.H., et al., 1995. Applications of silicate-melt inclusions to the study of magmatic volatiles. Magmas, Fluids Ore Deposits 23, 71–99.

Ludwig, W., King, A., Reischig, P., Herbig, M., Lauridsen, E.M., Schmidt, S., Proudhon, H., Forest, S., Cloetens, P., Du Roscoat, S.R., et al., 2009. New opportunities for 3D materials science of polycrystalline materials at the micrometre lengthscale by combined use of X-ray diffraction and X-ray imaging. Mater. Sci. Eng.: A 524 (1–2), 69–76.

Ludwig, W., Schmidt, S., Lauridsen, E.M., Poulsen, H.F., 2008. X-ray diffraction contrast tomography: a novel technique for three-dimensional grain mapping of polycrystals. I. Direct beam case. Appl. Crystallogr. 41 (2), 302–309.

Matteson, T.L., Schwarz, S.W., Houge, E.C., Kempshall, B.W., Giannuzzi, L.A., 2002. Electron backscattering diffraction investigation of focused ion beam surfaces. J. Electron. Mater. 31 (1), 33–39.

McDonald, S.A., Reischig, P., Holzner, C., Lauridsen, E.M., Withers, P.J., Merkle, A.P., Feser, M., 2015. Non-destructive mapping of grain orientations in 3D by laboratory X-ray microscopy. Sci. Rep. 5 (1), 14665.

Metrich, N., Wallace, P.J., 2008. Volatile abundances in basaltic magmas and their degassing paths tracked by melt inclusions. Rev. Miner. Geochem. 69 (1), 363–402.

Milani, S., Nestola, F., Angel, R.J., Nimis, P., Harris, J.W., 2016. Crystallographic orientations of olivine inclusions in diamonds. Lithos 265, 312–316.

Moore, L.R., Gazel, E., Tuohy, R., Lloyd, A.S., Esposito, R., Steele-MacInnis, M., Hauri, E.H., Wallace, P.J., Plank, T., Bodnar, R.J., 2015. Bubbles matter: An assessment of the contribution of vapor bubbles to melt inclusion volatile budgets. Am. Mineral. 100 (4), 806–823.

Mourey, A.J., Shea, T., 2019. Forming olivine phenocrysts in basalt: a 3D characterization of growth rates in laboratory experiments. Front. Earth Sci. 7, 300.

Nimis, P., Angel, R.J., Alvaro, M., Nestola, F., Harris, J.W., Casati, N., Marone, F., 2019. Crystallographic orientations of magnesiochromite inclusions in diamonds: what do they tell us? Contrib. Miner. Pet. 174 (4), 29.

Niverty, S., Sun, J., Williams, J., Bachmann, F., Gueninchault, N., Lauridsen, E., Chawla, N., 2019. A forward modeling approach to high-reliability grain mapping by laboratory diffraction contrast tomography (labdct). Jom (8), 2695–2704.

Pamukcu, A.S., Gualda, G.A., Bégué, F., Gravley, D.M., 2015. Melt inclusion shapes: Timekeepers of short-lived giant magma bodies. Geology 43 (11), 947–950.

Pamukcu, A.S., Gualda, G.A., Rivers, M.L., 2013. Quantitative 3D petrography using X-ray tomography 4: Assessing glass inclusion textures with propagation phase-contrast tomography. Geosphere 9 (6), 1704–1713.

Pankhurst, M.J., Gueninchault, N., Andrew, M., Hill, E., 2019. Non-destructive three-dimensional crystallographic orientation analysis of olivine using laboratory diffraction contrast tomography. Miner. Mag. 83 (5), 705–711.

Pankhurst, M.J., Oddershede, J., Jones, R.H., Thorley, D.M., Barbee, O.A., Vo, N.T., Dobson, K.J., Bodey, A., Eastwood, D., 2025. Using multimodal X-ray computed tomography to advance 3D petrography: A non-destructive investigation of olivine inside a carbonaceous chondrite. Am. Mineral. 110 (12), 1886–1897.

Poulsen, H.F., 2012. An introduction to three-dimensional X-ray diffraction microscopy. Appl. Crystallogr. 45 (6), 1084–1097.

Prior, D.J., Boyle, A.P., Brenker, F., Cheadle, M.C., Day, A., Lopez, G., Peruzzi, L., Potts, G., Reddy, S., Spiess, R., et al., 1999. The application of electron backscatter diffraction and orientation contrast imaging in the SEM to textural problems in rocks. Am. Mineral. 84 (11–12), 1741–1759.

Rasmussen, D.J., Plank, T.A., Wallace, P.J., Newcombe, M.E., Lowenstern, J.B., 2020. Vapor-bubble growth in olivine-hosted melt inclusions. Am. Mineral. 105 (12), 1898–1919.

Rawson, H., Naranjo, J.A., Smith, V.C., Fontijn, K., Pyle, D.M., Mather, T.A., Moreno, H., 2015. The frequency and magnitude of post-glacial explosive eruptions at Volcán Mocho-Choshuenco, southern Chile. J. Volcanol. Geotherm. Res. 299, 103–129.

Richard, A., Morlot, C., Créon, L., Beaudoin, N., Balistky, V.S., Pentelei, S., Dyja-Person, V., Giuliani, G., Pignatelli, I., Legros, H., et al., 2019. Advances in 3D imaging and volumetric reconstruction of fluid and melt inclusions by high resolution X-ray computed tomography. Chem. Geol. 508, 3–14.

Roedder, E., 1979. Origin and significance of magmatic inclusions. Bull. Mineral. 102 (5), 487–510.

Salas, P., Ruprecht, P., Hernández, L., Rabbia, O., 2021. Out-of-sequence skeletal growth causing oscillatory zoning in arc olivines. Nat. Commun. 12 (1), 4069.

Schiano, P., 2003. Primitive mantle magmas recorded as silicate melt inclusions in igneous minerals. Earth-Sci. Rev. 63 (1–2), 121–144.

Shea, T., Hammer, J.E., Hellebrand, E., Mourey, A.J., Costa, F., First, E.C., Lynn, K.J., Melnik, O., 2019. Phosphorus and aluminum zoning in olivine: contrasting behavior of two nominally incompatible trace elements. Contrib. Miner. Pet. 174 (10), 85.

Sobolev, A.V., 1996. Melt inclusions in minerals as a source of principle petrological information. Petrology 4 (3), 209–220.

Sobolev, A.V., Chaussidon, M., 1996. H2O concentrations in primary melts from supra-subduction zones and mid-ocean ridges: Implications for H2O storage and recycling in the mantle. Earth Planet. Sci. Lett. 137 (1–4), 45–55.

Sorby, H.C., 1858. On the microscopical, structure of crystals, indicating the origin of minerals and rocks. Q. J. Geol. Soc. 14 (1–2), 453–500.

Steele-MacInnis, M., Esposito, R., Moore, L.R., Hartley, M.E., 2017. Heterogeneously entrapped, vapor-rich melt inclusions record pre-eruptive magmatic volatile contents. Contrib. Miner. Pet. 172 (4), 18.

Sun, J., Dake, J.M., Oddershede, J., 2024. Grain structure evolution during heat treatment of a semisolid Al-Cu alloy studied with lab-based diffraction contrast tomography. Tomogr. Mater. Struct. 4, 100025.

Thornhill, H., Ferguson, D., Macente, A., Boschetty, F., Morgado, E., Harvey, J., 2026. Improving magmatic CO2 reconstruction using X-ray computed tomography to accurately quantify melt inclusion volumes and geometries. Volcanica 9 (1), 153–174. http://dx.doi.org/10.30909/vol/kppy1830.

Timms, N.E., Reddy, S.M., Gerald, J.D.F., Green, L., Muhling, J.R., 2012. Inclusion-localised crystal-plasticity, dynamic porosity, and fast-diffusion pathway generation in zircon. J. Struct. Geol. 35, 78–89.

Wallace, P.J., Plank, T., Bodnar, R.J., Gaetani, G.A., Shea, T., 2021. Olivine-hosted melt inclusions: a microscopic perspective on a complex magmatic world. Annu. Rev. Earth Planet. Sci. 49 (1), 465–494.

Welsch, B., Faure, F., Famin, V., Baronnet, A., Bachèlery, P., 2013. Dendritic crystallization: a single process for all the textures of olivine in basalts? J. Petrol. 54 (3), 539–574.

Welsch, B., Faure, F., First, E.C., 2023a. Reappraising crystallization kinetics with overgrowth chronometry: an in situ study of olivine growth velocities. J. Petrol. 64 (8), egad055.

Welsch, B., First, E.C., Ruprecht, P., Jollands, M.C., 2023b. Olivine—the little green science machine. Elements 19 (3), 138–143.

West, G.D., Thomson, R.C., 2009. Combined EBSD/EDS tomography in a dual-beam FIB/FEG–SEM. J. Microsc. 233 (3), 442–450.

Wieser, P.E., Edmonds, M., Maclennan, J., Wheeler, J., 2020. Microstructural constraints on magmatic mushes under kīlauea volcano, hawaii. Nat. Commun. 11 (1), 14.

Wirth, R., 2009. Focused ion beam (FIB) combined with SEM and TEM: Advanced analytical tools for studies of chemical composition, microstructure and crystal structure in geomaterials on a nanometre scale. Chem. Geol. 261 (3–4), 217–229.

Withers, P.J., Bouman, C., Carmignato, S., Cnudde, V., Grimaldi, D., Hagen, C.K., Maire, E., Manley, M., Du Plessis, A., Stock, S.R., 2021. X-ray computed tomography. Nat. Rev. Methods Prim. 1 (1), 18.

Xing, C.M., Wang, C.Y., Charlier, B., Namur, O., 2022. Ubiquitous dendritic olivine constructs initial crystal framework of mafic magma chamber. Earth Planet. Sci. Lett. 594, 117710.

Xing, C.M., Wang, C.Y., Tan, W., 2017. Disequilibrium growth of olivine in mafic magmas revealed by phosphorus zoning patterns of olivine from mafic–ultramafic intrusions. Earth Planet. Sci. Lett. 479, 108–119.

Xu, W., Ferry, M., Mateescu, N., Cairney, J.M., Humphreys, F.J., 2007. Techniques for generating 3-D EBSD microstructures by FIB tomography. Mater. Charact. 58 (10), 961–967.